

## Measurement crosstalk between two phase qubits coupled by a coplanar waveguide

Fabio Altomare,<sup>1,\*</sup> Katarina Cicak,<sup>1</sup> Mika A. Sillanpää,<sup>2</sup> Michael S. Allman,<sup>1,3</sup> Adam J. Sirois,<sup>1,3</sup> Dale Li,<sup>1</sup> Jae I. Park,<sup>1</sup> Joshua A. Strong,<sup>1,3</sup> John D. Teufel,<sup>1</sup> Jed D. Whittaker,<sup>1,3</sup> and Raymond W. Simmonds<sup>1,†</sup>

<sup>1</sup>National Institute of Standards and Technology, 325 Broadway, Boulder, Colorado 80305, USA

<sup>2</sup>Low Temperature Laboratory, Aalto University, PO Box 15100, FI-00076 AALTO, Finland,

<sup>3</sup>University of Colorado, 2000 Colorado Avenue, Boulder, Colorado 80309-0390, USA

(Received 2 February 2010; revised manuscript received 24 July 2010; published 14 September 2010)

We investigate measurement crosstalk in a system with two flux-biased phase qubits coupled by a resonant coplanar waveguide cavity. After qubit measurement, the superconducting phase undergoes damped oscillations in a deep anharmonic potential producing a frequency chirped voltage or crosstalk signal. We show experimentally that a coplanar waveguide cavity acts as a bandpass filter that can significantly reduce the propagation of this crosstalk signal when the qubits are far off resonance from the cavity. The transmission of the crosstalk signal  $\propto(\omega_q C_x)^2$  can be further minimized by reducing the qubit frequencies and the coupling capacitance to the cavity. We model the large amplitude crosstalk signal and qubit response classically with results that agree well with the experimental data. We find that the maximum energy transferred by the crosstalk generating qubit roughly saturates for long energy relaxation times ( $T_1 > 100$  ns) while the delay time necessary for the crosstalk signal to propagate to the cavity scales linearly with  $T_1$ . Ultimately, the use of resonant cavities as coupling elements and crosstalk filters is extremely beneficial for future architectures incorporating many coupled qubits.

DOI: [10.1103/PhysRevB.82.094510](https://doi.org/10.1103/PhysRevB.82.094510)

PACS number(s): 85.25.Cp

In recent years, much effort has been spent fabricating superconducting circuits with embedded Josephson junctions (JJs) as a promising platform for developing a quantum computer. In particular, superconducting qubits,<sup>1</sup> broadly classified as charge, flux, and phase, have achieved coherence times<sup>2</sup> longer than  $7 \mu\text{s}$ , and single shot visibility<sup>3</sup> close to 90%. Various schemes have been devised to couple several qubits in a more complex circuit: coupling through JJs,<sup>4</sup> inductive coupling,<sup>5</sup> capacitive coupling,<sup>6,7</sup> and coupling through a resonant coplanar waveguide<sup>8–10</sup> (CPW) cavity. The quantum mechanical nature of CPW cavities has also been demonstrated by generating arbitrary Fock states through the use of a coupled phase qubit.<sup>11</sup> Additionally, a protocol for the preparation of arbitrary entangled states of two phase qubits and a CPW cavity has been developed.<sup>12</sup> Here, we focus on two flux-biased phase qubits<sup>13</sup> coupled through a CPW cavity<sup>9,10,12</sup> and we show that the CPW cavity plays a crucial role in the reduction in measurement crosstalk.<sup>9,10</sup>

Measurement crosstalk in coupled flux-biased phase qubits<sup>7,14</sup> results from their unique formation in a metastable region of a double-well potential and the measurement scheme used for determining the qubit state. The schematic of a typical phase qubit<sup>15</sup> circuit is shown in Fig. 1(a). The phase qubit is essentially a resonant LC circuit in parallel with a Josephson inductance,  $L_j(\varphi) = \Phi_0 / (2\pi I_0 \cos \varphi)$ , where  $\Phi_0$  is the flux quantum,  $I_0$  is the JJ critical current, and  $\varphi$  is the quantum phase difference across the junction. For a given external flux applied to the circuit loop of inductance  $L$ ,  $\varphi_e = 2\pi\Phi_e / \Phi_0$ , we have  $\varphi + [L/L_j(0)]\sin \varphi = \varphi_e$ . The potential energy as a function of  $\varphi$  and  $\varphi_e$  is presented in Figs. 1(b) and 1(c). With a relatively strong anharmonicity, the quantized energy levels in the left well can be individually addressed in the microwave region with transition frequencies between the lowest quantized state  $|0\rangle$  and the first excited state  $|1\rangle$ . The occupation probability of the qubit's first ex-

cited state is measured by applying a fast flux pulse or measure pulse (MP) that tilts the well for a few nanoseconds<sup>16</sup> so that the  $|1\rangle$  state (and higher levels) can tunnel through the barrier to the right well, as shown in Fig. 1(c). Because the phase qubit is formed in a metastable region of the potential, its “ground state” energy is naturally higher than the global ground state of the system. Upon tunneling, this additional

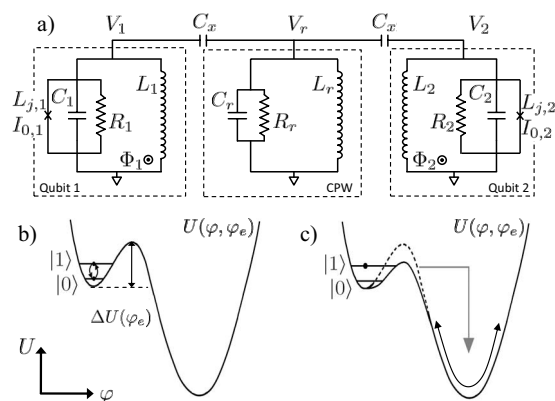


FIG. 1. (a) Equivalent electrical circuit for two flux-biased phase qubits coupled to a CPW cavity (modeled as a lumped element harmonic oscillator).  $C_i$  is the total capacitance for the  $i$ th qubit (or CPW cavity).  $L_i$  is the geometrical inductance.  $L_{j,i}$  is the Josephson inductance of the  $i$ th JJ.  $R_i$  models the dissipation in the system. (b)  $U(\varphi, \varphi_e)$  is the potential energy of a phase qubit as function of the superconducting phase difference  $\varphi$  across the JJ and the dimensionless external flux bias  $\varphi_e = 2\pi\Phi_e / \Phi_0$ .  $\Delta U(\varphi_e)$  is the difference between the local potential maximum and the local potential minimum in the left well at the flux bias  $\varphi_e$ . (c) During the MP, the potential barrier  $\Delta U(\varphi_e)$  between the two wells is lowered for a few nanoseconds allowing the  $|1\rangle$  state to tunnel into the right well where it will (classically) oscillate and lose energy due to dissipation.

energy is released so that the phase of the qubit undergoes large (roughly classical) oscillations in the deeper right well. Following the MP and a wait period, the flux is adjusted to form a symmetric double-well potential. After tens of microseconds, when the system has relaxed due to dissipation, a dc superconducting quantum interference device (SQUID) detects the flux in the qubit loop, allowing us to discriminate between the two circulating current states where the phase relaxed either in the left well or in the right well. These correspond to the qubit states  $|0\rangle$  if the qubit did not tunnel and  $|1\rangle$  if the qubit did tunnel.

The oscillations of the qubit phase in the right well produce an oscillating voltage<sup>17</sup> across the JJ with a relatively large size, representing roughly hundreds of microwave quanta. This voltage signal can excite any devices coupled to the qubit when their resonant frequency matches that of the oscillation. Because of dissipation, the oscillations in the right anharmonic potential well produce a signal with changing amplitude and frequency, a “chirped” pulse that can sample a frequency range spanning nearly 10 GHz. With direct capacitive coupling between two phase qubits,<sup>7</sup> this process results in the second qubit being excited over its metastable barrier whenever the first qubit is measured in the  $|1\rangle$  state. Due to the nonlinear dynamics of the system at the particular qubit flux biases chosen and the qubit dissipation rates, there is a finite delay time between the tunneling of the first qubit and the excitation of the second qubit. It was found that the loss of qubit information due to measurement crosstalk could be avoided by measuring the two qubits within  $\sim 2$  ns or essentially simultaneously.<sup>7</sup> A classical description of the qubit dynamics was found to sufficiently model the observed measurement crosstalk behavior.<sup>7,14</sup> Unfortunately, the excess energy released during a tunneling event is unavoidable so that measurement crosstalk could be a serious problem for directly coupling many metastable phase qubits.

The situation is quite different if two phase qubits are coupled through a CPW cavity. Here, we show explicitly both experimentally and theoretically (following Ref. 14) that the CPW cavity acts as a bandpass filter<sup>9,10</sup> and the second qubit is only excited when it is on resonance with the CPW cavity. This suggests a simple and effective way to reduce the measurement crosstalk between coupled phase qubit devices. Recently the beneficial features of this circuit have been used to verify the violation of Bells inequality with phase qubits.<sup>10</sup>

The device we use has already been described elsewhere<sup>12,18</sup> and consists of two flux-biased phase qubits capacitively coupled through a 7 mm open-ended coplanar waveguide whose half-wave resonant mode frequency is  $\omega_r/2\pi \approx 8.9$  GHz. Figure 1(a) shows the equivalent electrical circuit for the device. The dissipation in the circuit is modeled using the resistively shunted junction model.<sup>19</sup> The CPW cavity, with characteristic impedance  $Z_r \approx 50 \Omega$ , is equivalent to a lumped element resonator when close to resonance with an inductance  $L_r = 2Z_r/\pi\omega_r \approx 570$  pH and capacitance  $C_r = \pi/2\omega_r Z_r \approx 0.56$  pF. The lifetime of an excitation in the CPW cavity<sup>18</sup> is  $T_{1,r} \approx 1 \mu\text{s}$ , which yields  $R_r = T_{1,r}/C_r = 1.8$  M $\Omega$ . The qubits’ parameters are:  $L_1 = 690$  pH,  $C_1 = 0.7$  pF,  $I_{0,1} = 0.8 \mu\text{A}$ ,  $T_{1,1} = 170$  ns,

$R_1 = 240$  k $\Omega$ , and  $L_2 = 690$  pH,  $C_2 = 0.7$  pF,  $I_{0,2} = 0.95 \mu\text{A}$ ,  $T_{1,2} = 70$  ns,  $R_2 = 100$  k $\Omega$ , with  $C_x = 6.2$  fF providing a coupling strength  $2g/2\pi = (\omega_r/2\pi)C_x/\sqrt{C_r C_i} \sim 90$  MHz for both qubits,  $i = 1, 2$ . As discussed in Ref. 12, the resonant frequency of both qubits exhibits an avoided crossing at the CPW cavity frequency near 8.9 GHz. For the first qubit this happens at a flux  $\bar{\varphi}_1 = 0.82\varphi_{c1}$  and for the second at a flux  $\bar{\varphi}_2 = 0.842\varphi_{c2}$ . For the  $i$ th qubit,  $\varphi_{ci} = 2\pi\Phi_{ci}/\Phi_o$  is the critical flux where the left well of Fig. 1(b) disappears.

For our experiment, we use a MP to measure the tunneling probability  $P_{11}$  of the second (first) qubit after we purposely induce a tunneling event in the first (second) qubit using its MP. This forced tunnel event generates a crosstalk signal with 100% probability, allowing us to always measure  $P_{11}$ . Sweeping the time delay between the two MPs and measuring the qubit response allows us to determine<sup>7,9,12</sup> the optimal timing for “simultaneous measurement,” calibrating the different cabling and instrumental delays from the room-temperature equipment to the two cold qubits. Simultaneous measurement has been shown to be an effective method for reducing the strength of the measurement crosstalk process, producing the minimum crosstalk response.<sup>7,12,20</sup> Next, unlike previous measurements, we maximize the crosstalk response by incorporating an approximately  $\sim 50$  ns measurement delay between crosstalk generation with one qubit and crosstalk detection with the other qubit. In Figs. 2(a) and 2(c), we display the “measurement crosstalk,” defined as the measured tunneling probability  $P_{11}$  of the detection qubit in the presence of the crosstalk signal minus the residual tunneling probability out of the zero state without crosstalk, as a function of the bias fluxes applied to the two qubits. Here, the detection MP is calibrated to measure the tunneling probability of the  $|1\rangle$  state. Note that this choice will inevitably include contributions from higher energy states  $|n \geq 1\rangle$  that may have been excited by the chirped crosstalk signal.

When the detection qubit is off resonance, the minimum measurement crosstalk is 4% and 6% for the second and first qubit, respectively. The probability of finding the second (first) qubit has tunneled as a result of measurement crosstalk is an order of magnitude larger than the minimum value only in a region around  $\varphi_2/\varphi_{c2} \approx \bar{\varphi}_2/\varphi_{c2} = 0.842$  ( $\varphi_1/\varphi_{c1} \approx \bar{\varphi}_1/\varphi_{c1} = 0.82$ ) where the resonant frequency of the second (first) qubit is close to the CPW cavity frequency. The data clearly shows the cavities ability to filter the crosstalk signal. The insets show the response after averaging the curves over the horizontal axis. For comparison, the solid triangle in (a) and (b) represents the crosstalk response ( $\sim 2\%$ ) when the qubits are on resonance with the cavity and measured simultaneously.<sup>12</sup> The simultaneous measurement technique clearly avoids crosstalk even when the crosstalk signal can propagate through the cavity. As discussed later, further investigation is necessary to uncover the source of the residual crosstalk response.

There are a number of factors that must be taken into account when comparing measurement crosstalk for different phase qubit systems. First, the characteristics of the chirped crosstalk pulse depend to some degree on the qubit design parameters, which determine the shape of the anharmonic potential, the qubit operation point, and the energy relaxation times ( $T_1$ ) of the components. Second, the crosstalk sig-

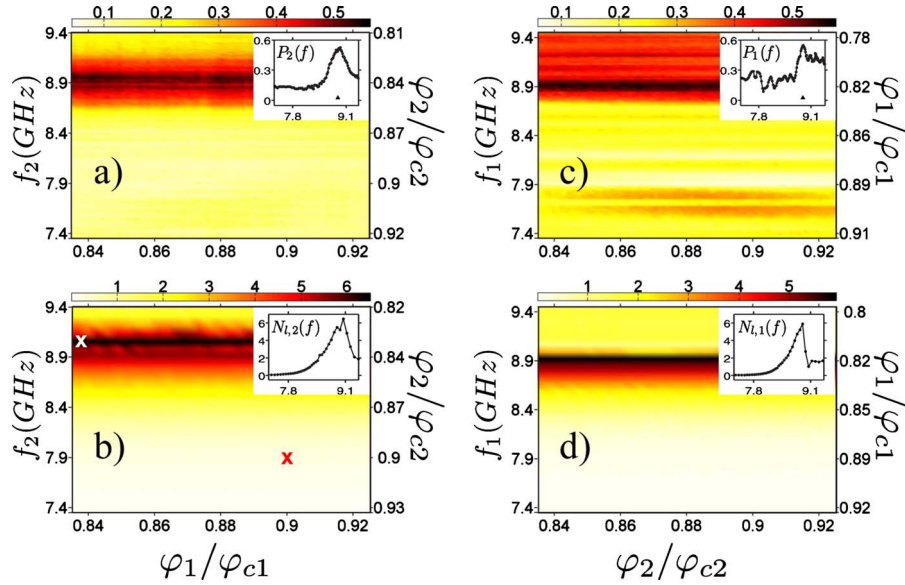


FIG. 2. (Color online) The crosstalk response with frequency. The insets show the response after averaging the curves over the horizontal axis. The single solid triangle in (a) and (b) represents the crosstalk response ( $\sim 2\%$ ) when the qubits are on resonance with the cavity and measured simultaneously. (a) Measurement crosstalk for qubit 2, after qubit 1 has already tunneled as a function of the (dimensionless) flux applied to the qubits. The measurement delay between crosstalk generation and detection was 56 ns. The left ordinate displays the resonant frequency as measured from the qubit spectroscopy. The right ordinate displays the ratio between the applied flux and the critical flux for qubit 2. (b) Simulation results showing the ratio ( $N_i$ ) between the maximum energy acquired by the second qubit and its resonant frequency (in the left well) as a function of the flux applied to the qubits. The left ordinate displays the oscillation frequency as determined from the fast Fourier transform of the energy of qubit 2. The right ordinate displays the ratio between the applied flux and the critical flux for qubit 1. Temporal traces corresponding to the two  $x$ 's are displayed in Fig. 3. (c) Measurement crosstalk for qubit 1, after qubit 2 has already tunneled. The measurement delay between crosstalk generation and detection was 34 ns. (d) Simulated results for qubit 1, after qubit 2 has already tunneled.

nal experiences a delay time during propagation. Simultaneous measurement<sup>7</sup> is a technique that has been used to minimize measurement crosstalk. And finally, and most importantly, the ability of the crosstalk signal to propagate depends on the coupling strengths between the coupled systems and the frequency of operation.<sup>14</sup> A simple analysis of our circuit shows that off resonance from the cavity, the transmission of the crosstalk signal roughly scales inversely with the square of the impedance of the coupling capacitor or proportional to  $(\omega_q C_x)^2$ , where  $\omega_q$  is the angular frequency of the qubits. Thus, reducing the frequency of operation and the coupling capacitance  $C_x$  reduces measurement crosstalk.

The first crosstalk measurements<sup>7</sup> with two directly coupled phase qubits were performed with similar design parameters as our experiment, a similar coupling capacitor ( $C_x \sim 6$  fF), and a similar operation frequency ( $\sim 8.65$  GHz), but with a reduced energy relaxation time ( $T_1 \sim 25$  ns). Here, for simultaneous measurement of the two qubits on resonance with each other, measurement crosstalk of approximately  $\sim 6\%$  was determined by the maximum probability amplitude  $P_{11}$  (minus background tunneling) that both qubits tunneled after a  $\pi$ -pulse excited only one of the qubits. In a similar two-qubit experiment,<sup>20</sup> measurement crosstalk of approximately  $\sim 10\%$  was determined for qubits with  $T_1 \sim 130$  ns coupled with a capacitor  $C_x \sim 3$  fF, operated on resonance (5.1 GHz) and measured simultaneously. Away from the cavity resonance, our results show an improvement in measurement crosstalk even with

improved energy relaxation times, larger coupling capacitors and without simultaneous measurement, regardless of the resonance condition of the two qubits. An impressively low level of measurement crosstalk was reported by Ansmann *et al.*<sup>10</sup> by operating their high fidelity qubits sufficiently detuned ( $\sim 500$  MHz) from a CPW cavity ( $\sim 7.2$  GHz) that was weakly coupled ( $g/\pi \sim 30$  MHz) to the qubits. With a ( $\sim 2$  GHz) lower frequency system and coupling strengths a factor of 3 smaller than ours, they were able to minimize the measurement crosstalk to  $< 1\%$ , consistent with the  $(\omega_q C_x)^2$  scaling of the coupling impedances.

To provide a qualitative description of these results, we perform simulations of this system of two qubits coupled by a cavity [Fig. 1(a)]. Once the crosstalk generating qubit has tunneled, the qubit acts like a weakly anharmonic oscillator that can initially contain hundreds of quanta, allowing us to model the behavior classically. Following Kofman *et al.*,<sup>14</sup> we write the Lagrangian as

$$\mathcal{L} = \frac{1}{2}C_1V_1^2 + \frac{1}{2}C_2V_2^2 + \frac{1}{2}C_rV_r^2 + \frac{1}{2}C_x(V_1 - V_r)^2 + \frac{1}{2}C_x(V_r - V_2)^2 - U_1(\phi) - U_2(\phi) - \frac{\Phi_r^2}{2L_r}, \quad (1)$$

where  $\Phi_r^2/2L_r = L_r I_r^2/2$  is the potential energy in the CPW cavity and the potential energy of the qubit is



$$U_i = E_{L,i} \left[ \frac{1}{2} (\varphi_i - \varphi_{e,i})^2 - \frac{L_i}{L_{J,i}} \cos \varphi_i \right] \quad (2)$$

with  $E_{L,i} = (\Phi_0/2\pi)^2/L_i$ . The dimensionless flux,  $\varphi_{e,i} = 2\pi\Phi_i/\Phi_0$ , determines the profile of the potential energy of the qubit. Using the Josephson relations (to substitute  $V_i$  with  $\dot{\varphi}_i$ ) and deriving the equations of motion, after including the damping terms, we obtain<sup>21</sup>

$$\begin{aligned} C_1 \ddot{\varphi}_1 + C_x (\ddot{\varphi}_1 - \ddot{\varphi}_r) &= - \left( \frac{2\pi}{\Phi_0} \right)^2 \frac{\partial U_1}{\partial \varphi_1} - \frac{1}{R_1} \dot{\varphi}_1, \\ C_r \ddot{\varphi}_r + C_x (\ddot{\varphi}_1 - \ddot{\varphi}_r) + C_x (\ddot{\varphi}_r - \ddot{\varphi}_2) &= - \frac{\varphi_r}{L_r} - \frac{\dot{\varphi}_r}{R_r}, \\ C_2 \ddot{\varphi}_2 + C_x (\ddot{\varphi}_r - \ddot{\varphi}_2) &= - \left( \frac{2\pi}{\Phi_0} \right)^2 \frac{\partial U_2}{\partial \varphi_2} - \frac{1}{R_2} \dot{\varphi}_2, \end{aligned} \quad (3)$$

where  $\varphi_r = 2\pi\Phi_r/\Phi_0$ . Note that, in contrast to Refs. 7 and 14, we solve this system of coupled equations completely, including the ‘‘backaction’’ experienced by the crosstalk generating qubit when it interacts with the cavity. This will have important consequences (discussed later) regarding the dependence of measurement crosstalk amplitude and propagation delay on the crosstalk generating qubit’s lifetime in the deep right well ( $\bar{T}_1$ ).

We adjust the initial conditions of the simulation in order to capture the main features of the crosstalk generation process. In the experiment, when the MP is applied to the crosstalk generating qubit, the flux approaches the critical value over a short period of time, so that the ground state tunnels with unit probability. For the simulation, we assume a potential-energy shape for the crosstalk generating qubit given by an applied flux equal to  $0.95\varphi_c$ . We set the kinetic energy to zero ( $\dot{\varphi}_1=0$ ), the initial phase value to be in the right well below the local maximum [Fig. 1(b)] by an amount equal to  $\sim 0.2\Delta U(\varphi_e)$  for the flux bias value  $\varphi_e$ . The zero of the potential energy is defined at the bottom of the right well. These conditions ensure proper evolution dynamics<sup>14</sup> while incorporating the initial energy of the generating qubit at various flux biases. The cavity and the crosstalk detection qubit begin with zero kinetic energy ( $\dot{\varphi}_r=\dot{\varphi}_2=0$ ) and have zero potential energy, defined at the bottom of the left well. We assume that the decay rate in the right well ( $\bar{T}_1$ ) is the same as in the left well ( $T_1$ ), although there is evidence (discussed later) that it should be smaller,<sup>14,22</sup> and perform the simulation for a duration  $\sim 3T_1$ , after which the phase has relaxed to rest. We have checked that small variations in these initial conditions do not meaningfully affect the results of our simulations.<sup>14</sup>

From these initial conditions the phase of the crosstalk generating qubit (classically) undergoes damped oscillations in the anharmonic right well. Because of the anharmonicity of the potential, when the amplitude of the oscillations is large, the frequency of the oscillations is lower than the cavity frequency. As the oscillator loses energy from dissipation, the oscillation frequency increases. When the frequency matches that of the CPW cavity, energy can be transferred to

the CPW cavity. If the detection qubit’s frequency matches that of the CPW cavity, then the cavity’s excitation can be transferred to the qubit. As done previously,<sup>7,14</sup> we classically determine the excitation level of the detection qubit and draw a qualitative correspondence between these values and the experimental results for the probability amplitude of the measurement crosstalk. The maximum excitation level acquired by the detection qubit in the shallow well is determined by the ratio ( $N_l$ ) between the maximum energy acquired and  $\hbar\omega_p$ , where  $\omega_p$  is the plasma frequency (in the left well) of the detection qubit. We perform these simulations for various fluxes bias values applied to each qubit in accordance with the experimental conditions.

As can be seen from Fig. 2(b), the crosstalk is maximum at a flux  $\varphi_2/\varphi_{c2} \sim 0.837$ , where the detection qubit’s frequency is approximately 8.97 GHz, determined by taking the fast Fourier transform of the oscillations in energy over time [see Figs. 3(a)–3(c)]. Reversing the roles of the two qubits, we find that for the first qubit the crosstalk is maximum at a flux  $\varphi_1/\varphi_{c1} \sim 0.825$ , corresponding to an excitation frequency of approximately 8.84 GHz [Fig. 2(d)]. These values were determined for qubit 2 (qubit 1) by performing a Gaussian fit of  $N_l$  versus flux (or frequency) after averaging over the span of flux values for qubit 1 (qubit 2). Notice that the crosstalk transferred to qubit 2 (qubit 1) is flux independent of qubit 1 (qubit 2) and substantial only when the cavity frequency matches the frequency of qubit 2 (qubit 1). The results of the simulations are in good agreement with the experimental data.

To gain additional insight into the dynamics of the system, we plot the time evolution of the energy for the qubits and the CPW cavity [Figs. 3(a)–3(c)] for two different sets of fluxes in the two qubits. At  $\varphi_1/\varphi_{c1}=0.9$  and  $\varphi_2/\varphi_{c2}=0.9$  [red x in Fig. 2(b)] the first qubit decays exponentially for a time  $t \lesssim 125$  ns [Figs. 3(a)–3(c), red]. At  $t \approx 125$  ns, there is a downward jump in the energy of the first qubit while the energy of the CPW cavity exhibits an upward jump. At this time, the frequency of oscillation in the right well matches the CPW cavity resonant frequency, so part of the qubit’s energy is transferred to the CPW cavity. We can define a propagation time delay  $\tau_d$  (for the cavity) that represents the time duration necessary for the cavity to first absorb half its maximum energy. In this case, we have  $\tau_d \sim 125$  ns, but the second qubit is not on resonance with the CPW cavity, so it does not absorb the energy deposited in the cavity from the crosstalk signal.

At  $\varphi_1/\varphi_{c1}=0.835$  and  $\varphi_2/\varphi_{c2}=0.836$  [white x in Fig. 2(b)], the dynamics of the first qubit and the CPW cavity are essentially unchanged, except that the CPW cavity frequency is matched at a different time, with a different propagation time delay ( $\tau_d \sim 103$  ns) because the first qubit starts at a lower energy in the deep right well [Figs. 3(a)–3(c), black]. However, in this case, the second qubit is on resonance with the CPW cavity and is therefore excited to an energy  $N_l \sim 6$ .

Next, assuming qubit 1 generates the crosstalk signal and qubit 2 detects it [Figs. 2(a) and 2(c)], we run our simulation for different  $\bar{T}_1$  times in the right well focusing our attention on (see Fig. 4): (a) the maximum energy of the cavity with

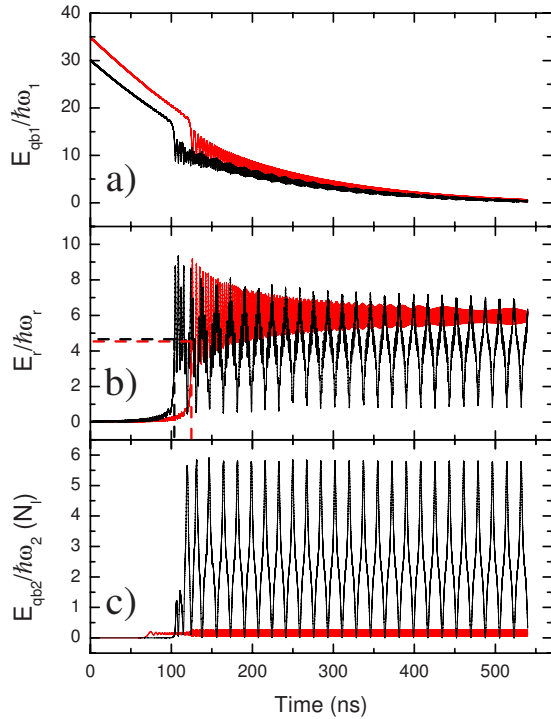


FIG. 3. (Color online) Simulated energy for (a) the first qubit, (b) the CPW cavity, and (c) the second qubit. The energy is measured in units of  $\hbar\omega_i$ , where  $\omega_i/2\pi$  is the plasma frequency for the well of oscillation: the first qubit oscillates in its deep right well, the cavity oscillates in its parabolic well, and the second qubit oscillates in its shallow left well. [Red, corresponding to the red x of Fig. 2(b).]  $\varphi_1=0.9\varphi_{c1}$  and  $\varphi_2=0.9\varphi_{c2}$ . The first qubit decays exponentially until  $t \approx 125$  ns. At this time, the oscillation frequency in the right well matches the CPW cavity resonant frequency and the qubit transfers part of its energy to the CPW cavity. Here the propagation time delay is  $\tau_d \sim 125$  ns (see text) as indicated by the dashed lines in (b). In this case, the second qubit is off resonance from the cavity and is therefore minimally affected by the crosstalk signal. [Black, corresponding to the white x of Fig. 2(b).]  $\varphi_1=0.835\varphi_{c1}$  and  $\varphi_2=0.836\varphi_{c2}$ . In this case, the first qubit transfers energy to the CPW cavity with a propagation time delay of  $\tau_d \sim 103$  ns as indicated by the dashed lines in (b). This shorter value is due to a lower initial energy or starting position in the deep right well. At this flux the second qubit is on resonance with the cavity and therefore excited to an energy  $N_l \sim 6$ .

the second qubit off resonance, (b) the propagation delay time ( $\tau_d$ ) for the cavity, and (c) the maximum energy transferred to qubit 2, the crosstalk detection qubit, when on resonance with the cavity.

Figure 4(a) shows that the maximum energy acquired by the cavity has a much weaker dependence on  $\bar{T}_1$  than that reported in Kofman *et al.*<sup>14</sup> We have verified that the simulation results do not change significantly when qubit 2 is on resonance with the cavity. The weak dependence on  $\bar{T}_1$  can be understood fairly easily after looking back at our discussion of Fig. 3. When the frequency of the oscillations in the qubit's right well matches the cavity frequency, the qubit transfers part of its energy to the cavity. This energy transfer subsequently decreases the amplitude of the qubit's oscillations and, due to the anharmonicity of the deep right well,

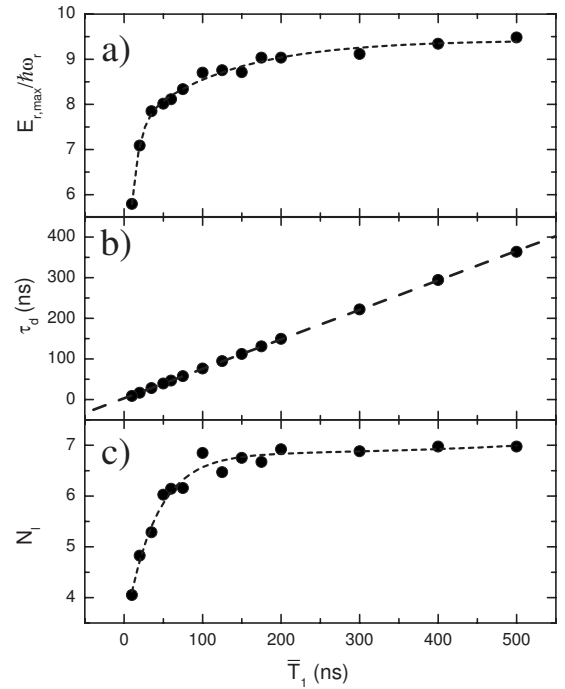


FIG. 4. (a) Maximum cavity energy as function of  $\bar{T}_1$  of the crosstalk generating qubit with  $\varphi_1=0.9\varphi_{c1}$  and  $\varphi_2=0.9\varphi_{c2}$ . The dots are the results of the simulation while the dashed line is a guide to the eyes. Similar results have been obtained with the second qubit on resonance. (b) Cavity propagation delay time ( $\tau_d$ ) as function of  $\bar{T}_1$  for  $\varphi_1=0.9\varphi_{c1}$  and  $\varphi_2=0.9\varphi_{c2}$ . Similar results have been obtained with the second qubit on resonance. The dashed line is a linear fit to the data (dots),  $\tau_d=0.72\bar{T}_1+3.2$  ns. (c) Maximum energy of the crosstalk detection qubit  $N_l$  as function of  $\bar{T}_1$ . The dots are the results of the simulation while the dashed line is a guide to the eyes.

quickly *increases* its oscillation frequency, moving it off resonance from the cavity. For  $\bar{T}_1 < 100$  ns, this interaction is so rapid that the cavity cannot be efficiently excited. For  $\bar{T}_1 > 100$  ns the qubit transfers energy more effectively but further increasing  $\bar{T}_1$  by a factor of 5 only mildly increases ( $\leq 10\%$ ) the maximum energy transferred to the cavity. This increase is much smaller than previously suggested<sup>14</sup> because we have included [in Eq. (3)] the coupled interactions in our simulations allowing for backaction effects.

Figure 4(b) shows the dependence of the propagation time delay  $\tau_d$  as a function of  $\bar{T}_1$ . We found it is easier to uniquely determine  $\tau_d$  based on the cavity's response rather than the detection qubit's response because the cavity dynamics (particle in an harmonic potential) are much simpler than the qubit dynamics (particle in an anharmonic potential). As expected, the longer  $\bar{T}_1$ , the longer the propagation delay time  $\tau_d$ . We have found that  $\tau_d$  depends linearly on  $\bar{T}_1$ . This can be understood in the following way. The frequency of oscillation in the deep right well is a function of amplitude or energy. Upon tunneling, the initial (potential) energy  $E_i$  decays exponentially with a characteristic time  $\bar{T}_1$ . At a particular energy  $E_c$ , the oscillation frequency matches that of the

cavity. Since the propagation delay time is dominated by the time it takes to reach  $E_c$ , we have  $\tau_d \approx \ln(E_i/E_c)\bar{T}_1$ . For our circuit parameters and the flux bias chosen, we have  $\tau_d = 0.72\bar{T}_1 + 3.6$  ns, giving  $E_i/E_c \sim \exp(0.72) \sim 2$ , consistent with the results shown in Figs. 3(a) and 3(b). Our simulations also suggest that for our experiment, the lifetime in the deep right well is  $\bar{T}_1 \lesssim 50$  ns, smaller than the lifetime  $T_1$  of the qubit's first excited state  $|1\rangle$  (Fig. 2). We have verified that the simulation results do not change significantly when qubit 2 is on resonance with the cavity.

With the second qubit on resonance with the cavity, Fig. 4(c) shows the maximum energy of the second qubit as function of  $\bar{T}_1$  of the first qubit. A quick comparison between Figs. 4(a) and 4(c) shows that the behavior of the maximum energy of the crosstalk detection qubit closely follows the maximum cavity energy. This is expected since the second qubit is excited *only* by the cavity. Since the cavity is harmonic, exchanging energy with the qubit does not alter its oscillating frequency and the two will oscillate out of phase with respect to each other [see Figs. 3(b) and 3(c)] as they exchange energy.

We chose to follow a simple modeling approach<sup>7,14</sup> that provides a qualitative comparison for the amplitude of the measurement crosstalk and also generates a quantitative agreement with respect to the frequency response of the system to the crosstalk signal. We have extended our model to include the backaction among the three coupled systems. Although the experimental situation is more complicated by the actual presence of the MP, we still find good agreement between the classical simulation and the experimental results.

We have experimentally investigated measurement crosstalk between two metastable phase qubits coupled through a resonant CPW cavity. We have used a classical approach to fully simulate the coupled interaction of these three systems including backaction. We have confirmed that the resonant cavity acts as a bandpass filter reducing the detrimental affects of measurement crosstalk as long as the qubits are sufficiently detuned from the cavity resonance.<sup>9,10</sup> The solution of coupled equations of motion [Eq. (3)] allowed us to show that the dependence of the measurement crosstalk amplitude on  $\bar{T}_1$  is weaker than previously suspected.<sup>14</sup> In addition, the propagation delay time  $\tau_d$  grows linearly with  $\bar{T}_1$ . The transmission of the crosstalk signal  $\propto (\omega_q C_x)^2$  can be further minimized by reducing the frequency of the qubits and the coupling capacitance to the cavity.

In order to properly characterize the time dynamics of the crosstalk signal and confirm the theory curves in Figs. 3 and 4 a different measurement scheme is necessary. With the current measurement/readout scheme, the qubit is measured by a quick change in flux (the MP) and readout is performed roughly 20  $\mu$ s later by an inductively coupled dc SQUID. With this scheme, it is difficult to clearly identify the arrival times of the crosstalk signal. For example, there is no way to distinguish between the two following scenarios: (a) the

crosstalk signal reaches the crosstalk detecting qubit, excites the qubit to the first excited level. Within the qubit energy decay time, the MP arrives at the crosstalk detecting qubit enhancing the tunneling probability of the  $|1\rangle$  state so that the qubit tunnels to the right well. After  $\sim 20$   $\mu$ s the readout SQUID detects the qubit in the right well signifying that the qubit was in the  $|1\rangle$  state when the MP arrived. (b) The MP arrives at the crosstalk detecting qubit enhancing the tunneling rate for the excited state but because the qubit is in the ground state no tunneling event occurs. A short time later, the crosstalk signal arrives at the crosstalk detecting qubit and then excites the qubit to higher energy levels in the shallow left well. With these higher levels having an exponentially higher tunneling rate, a tunneling event occurs to the right well without the presence of the MP. After  $\sim 20$   $\mu$ s, the readout SQUID detects the qubit in right well, *falsely* signifying that the qubit was in the  $|1\rangle$  state when the MP arrived, but clearly indicating the presence of the crosstalk signal. Other possible scenarios can be envisioned that disrupt our ability to clearly measure how the detection qubit responds to the crosstalk signal over time.

The difficulty here is that multiple conditions can lead to a tunneling event (the “measurement”) and the readout does not occur until much later. Using a different measurement/readout technique that measures and reads out the qubit state at the same time, such as fast dispersive single-shot measurements,<sup>23</sup> would clearly provide the ability to readout the state of the crosstalk detecting qubit at any moment in time in order to capture the dynamics of the system. This would allow a direct test of the crosstalk phenomenon and provide a way to compare our simplified assumptions in the theory with the complexity of the experiment. We are working toward a fast dispersive measurement/readout of phase qubits at this time.

In the future, it may be interesting to investigate the transfer of the crosstalk signal through an anharmonic resonant cavity whose frequency versus amplitude characteristic may eliminate crosstalk completely. Simultaneous measurement, although effective in some cases, cannot protect crosstalk from destroying ancillary, computational, or feed-forward qubits still processing and not ready for measurement. Measurement crosstalk can be a problem for other systems that rely on a switching process that can radiate crosstalk to other coupled systems during qubit measurement. Ultimately, future device architectures incorporating multiple qubits can benefit from the use of resonant cavities between the qubits to prevent measurement crosstalk. Improving fidelity and reducing errors during qubit measurement is crucial for the creation and use of multiqubit entangled states<sup>10,12,24</sup> and performing complex algorithms.

This work was financially supported by NIST. Contribution of the U.S. government, not subject to copyright. M.A.S. was supported by the Academy of Finland and by the ERC (Grant No. FP7-240387).

\*Present address: D-Wave Systems Inc., 100–4401 Still Creek Drive, Burnaby, British Columbia, Canada V5C 6G9.

†simmonds@boulder.nist.gov

<sup>1</sup>For a recent review see J. Clarke and F. K. Wilhelm, *Nature (London)* **453**, 1031 (2008), and references therein.

<sup>2</sup>A. Wallraff, D. I. Schuster, A. Blais, L. Frunzio, J. Majer, M. H. Devoret, S. M. Girvin, and R. J. Schoelkopf, *Phys. Rev. Lett.* **95**, 060501 (2005).

<sup>3</sup>O. Astafiev, Y. A. Pashkin, T. Yamamoto, Y. Nakamura, and J. S. Tsai, *Phys. Rev. B* **69**, 180507 (2004); A. Lupascu, E. F. C. Driessen, L. Roschier, C. J. P. M. Harmans, and J. E. Mooij, *Phys. Rev. Lett.* **96**, 127003 (2006); M. Steffen, M. Ansmann, R. McDermott, N. Katz, R. C. Bialczak, E. Lucero, M. Neeley, E. M. Weig, A. N. Cleland, and J. M. Martinis, *ibid.* **97**, 050502 (2006).

<sup>4</sup>M. Grajcar, A. Izmalkov, S. H. van der Ploeg, and S. Linzen, E. Il'ichev, T. Wagner, U. Hübner, H. Meyer, A. Maassen van den Brink, S. Uchaikin, and A. M. Zagoskin, *Phys. Rev. B* **72**, 020503 (2005).

<sup>5</sup>J. B. Majer, F. G. Paauw, A. C. Ter Haar, C. J. Harmans, and J. E. Mooij, *Phys. Rev. Lett.* **94**, 090501 (2005); A. O. Niskanen, K. Harrabi, F. Yoshihara, Y. Nakamura, and J. S. Tsai, *Phys. Rev. B* **74**, 220503(R) (2006); A. O. Niskanen, K. Harrabi, F. Yoshihara, Y. Nakamura, S. Lloyd, and J. S. Tsai, *Science* **316**, 723 (2007); M. S. Allman, F. Altomare, J. D. Whittaker, K. Cicak, D. Li, A. Sirois, J. A. Strong, J. D. Teufel, and R. W. Simmonds, *Phys. Rev. Lett.* **104**, 177004 (2010).

<sup>6</sup>Y. A. Pashkin, T. Yamamoto, O. Astafiev, Y. Nakamura, D. V. Averin, and J. S. Tsai, *Nature (London)* **421**, 823 (2003); A. J. Berkley, H. Xu, R. C. Ramos, M. A. Gubrud, F. W. Strauch, P. R. Johnson, J. R. Anderson, A. J. Dragt, C. J. Lobb, and F. C. Wellstood, *Science* **300**, 1548 (2003).

<sup>7</sup>R. McDermott, R. Simmonds, M. Steffen, K. Cooper, K. Cicak, K. Osborn, S. Oh, D. Pappas, and J. Martinis, *Science* **307**, 1299 (2005).

<sup>8</sup>J. Majer, J. M. Chow, J. M. Gambetta, J. Koch, B. R. Johnson, J. A. Schreier, L. Frunzio, D. I. Schuster, A. A. Houck, A. Wallraff, A. Blais, M. H. Devoret, S. M. Girvin, and R. J. Schoel-

kopf, *Nature (London)* **449**, 443 (2007).

<sup>9</sup>M. A. Sillanpää, J. I. Park, and R. W. Simmonds, *Nature (London)* **449**, 438 (2007).

<sup>10</sup>M. Ansmann, H. Wang, R. C. Bialczak, M. Hofheinz, E. Lucero, M. Neeley, A. D. O'Connell, D. Sank, M. Weides, J. Wenner, A. N. Cleland, and J. M. Martinis, *Nature (London)* **461**, 504 (2009).

<sup>11</sup>M. Hofheinz, H. Wang, M. Ansmann, R. C. Bialczak, E. Lucero, M. Neeley, A. D. O'Connell, D. Sank, J. Wenner, J. M. Martinis, and A. N. Cleland, *Nature (London)* **459**, 546 (2009).

<sup>12</sup>F. Altomare, K. Cicak, M. A. Sillanpää, M. Allman, A. Sirois, J. A. Strong, D. Li, J. Park, J. D. Whittaker, and R. W. Simmonds, *Nature Physics* (to be published 2010).

<sup>13</sup>R. W. Simmonds, K. M. Lang, D. A. Hite, S. Nam, D. P. Pappas, and J. M. Martinis, *Phys. Rev. Lett.* **93**, 077003 (2004).

<sup>14</sup>A. G. Kofman, Q. Zhang, J. M. Martinis, and A. N. Korotkov, *Phys. Rev. B* **75**, 014524 (2007).

<sup>15</sup>In the remainder, we will refer to the flux-biased phase qubit simply as a phase qubit.

<sup>16</sup>K. B. Cooper, M. Steffen, R. McDermott, R. W. Simmonds, S. Oh, D. A. Hite, D. P. Pappas, and J. M. Martinis, *Phys. Rev. Lett.* **93**, 180401 (2004).

<sup>17</sup>B. D. Josephson, *Rev. Mod. Phys.* **46**, 251 (1974).

<sup>18</sup>R. Simmonds, M. Allman, F. Altomare, K. Cicak, K. Osborn, J. Park, M. Sillanpää, A. Sirois, J. Strong, and J. Whittaker, *Quantum Inf. Process.* **8**, 117 (2009).

<sup>19</sup>T. Van Duzer and C. Turner, *Principles of Superconducting Circuits* (Elsevier, New York, 1981).

<sup>20</sup>M. Steffen, M. Ansmann, R. C. Bialczak, N. Katz, E. Lucero, R. McDermott, M. Neeley, E. M. Weig, A. N. Cleland, and J. M. Martinis, *Science* **313**, 1423 (2006).

<sup>21</sup>To speed up the calculations, the damping term for the CPW cavity and the second qubit have been omitted.

<sup>22</sup>J. A. Strong, Ph.D. Thesis, University of Colorado, 2010.

<sup>23</sup>F. Mallet, F. R. Ong, A. Palacios-Laloy, F. Nguyen, P. Bertet, D. Vion, and D. Esteve, *Nat. Phys.* **5**, 791 (2009).

<sup>24</sup>A. G. Kofman and A. N. Korotkov, *Phys. Rev. B* **77**, 104502 (2008).